53rd 3AF International Conference on Applied Aerodynamics
26 – 28 March 2018, Salon de Provence, France

FP09-AERO2018-faure

Simulation of the aeroelastic behavior of a possibly detached flow airfoil by a discrete vortex method

Thierry M. FAURE[(1)], Laurent DUMAS[(1)], Bertrand KIRSCH[(1)] and Olivier MONTAGNIER[(1)]
[(1)] *Centre de Recherche de l'Armée de l'air, École de l'Air, B.A. 701, 13661 Salon-de-Provence, France, thierry.faure@defense.gouv.fr*

ABSTRACT

The aeroelastic behavior of an airfoil results in a complex coupling between the elastic response of the structure and the dynamics of the flow. It can lead to the failure of a lifting surface which consequences could be catastrophic. Experiments and high-order computations contribute to the understanding of this phenomenon, but fast low-order methods are needed for engineering tasks. In the present work, we implement a loose fluid-structure coupling between a discrete-time vortex method, using a leading edge shedding criterion, and the structure motion equations. For each time step, the aerodynamic coefficients are first calculated before the computation of the motion of the structure. Flutter velocity is obtained with the same precision as unsteady standard method. The advantage of the method proposed is the ability to catch the limit cycle for velocities larger than flutter speed due to dynamic stall of the airfoil.

1. INTRODUCTION

The vibration and instability of lifting surfaces have been detected from the very beginning of aeronautics, because of their destructive consequences on structures leading to breaking and crashes. The flutter have been identified in the 1920s on the first fast airplanes, resulting in the use of more stiffen materials. However, if the consequences of this instability were noticed, their physical understanding remained unknown at that time.
The classical flutter is a dynamic instability resulting from the coupling between the first twisting mode and the first bending mode of the structure. The difficulty of its prediction lays in the estimate of the aerodynamic forces involved.
The fluid structure interaction mechanisms can be classified on the reduced frequency $f_r = T_f/T_s$ [1] with T_f the period of fluid motion and T_s the period of structure motion. If f_r is much larger than one, the structure is in a high frequency excitation regime (vibroacoustics) and acts as if it was moving in a steady fluid. If f_r is much smaller than one, the structure frequencies are low, corresponding to quasi-static aeroelasticity. If f_r is of the order of one, there is a tight fluid-structure coupling corresponding to present investigation.
Theories have been developed for the prediction of aerodynamic forces on a steady attached airfoil such as the thin airfoil theory [2, 3, 4], with very limited application. Quasi-steady flows are considered when, for each time, the instantaneous position of the structure results in a steady flow [1]. The velocity induced by the vertical translation of the structure is considered [5], which can be added to the angle of attack of the airfoil. Unsteady theories were initiated by Wagner [6] who calculated the lift of a wing with a rapid change of the angle of attack. A potential flow solution for a flat plane with low amplitude harmonic oscillations was developed by Theodorsen [7]. Other potential methods were developed [8, 9] but remained limited to attached flow configurations. Detached flow configurations were considered in the 1970s [10, 11, 12] introducing vortex shedding in the potential flow. The development of more powerful computers in this decade led flow simulations toward another way with the high-order resolution of Navier-Stokes equations with closure models. However, the potential methods remained used for a long time to solve aeroelastic issues, in particular the Doublet-Lattice Method [13] and the Vortex-Lattice Method [14].
On the other hand, for fluid dynamics prediction, discrete vortex methods came back in use recently as alternative low-order methods to classical high-order computational fluid dynamics (CFD), to address engineering issues with relevant accuracy. Discrete vortex methods where developed to model leading edge vortices in unsteady flows [15, 16, 17]. However, these methods are limited to start and stop criteria for the vortex shedding. This issue was addressed with the implementation of a leading edge suction parameter [18]. That criterion allows a wide range of applications for any airfoil geometry, with sharp or rounded leading

edges, and any arbitrary motion. Its robustness and its relative accuracy was demonstrated as long as a leading edge boundary layer separation occurs [19]. The Leading edge suction parameter Discrete Vortex Method (LDVM) algorithm is based, for each time step, on iterative schemes to obtain the circulation of the last generated vortices through a converging time consuming process.

Aeroelasticity issues require rapid and efficient method for engineering problems. Different frequency methods, *p*, *k*, *p-k* [5, 20, 21] are suitable to address these problems. However, the present coupling between the aeroelastic issue and LDVM requires a time solving. The fluid and structure equations are solved in a single code with a direct loose coupling [22].

In the paper, the discrete vortex method used is presented first. The fluid-structure interaction coupling equations are then introduced with the resolution method of Newmark. Results for a light aircraft [5] are discussed versus the upstream flow velocity, exhibiting a threshold velocity between convergent and divergent cases.

2. LEADING EDGE SUCTION PARAMETER DISCRETE VORTEX METHOD

The Leading edge suction parameter Discrete Vortex Method (LDVM) is based on the potential thin airfoil theory in unsteady flows, applicable for large values of the angle of attack [18]. It is built on the time-stepping approach of [23] with the addition of a criterion for the leading edge detachment.

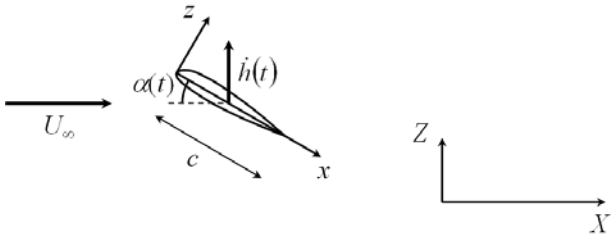

Figure 1. Airfoil motion and frames of reference.

In figure 1, the aerodynamic frame (X,Z) is fixed and the airfoil frame (x,z) sees an upstream velocity U_∞ aligned on the X axis with a time-dependant angle of attack $\alpha(t)$. A vertical motion $h(t)$ is considered along the Z axis. The fluid velocity components are respectively U and W in the aerodynamic frame and w is the velocity along z in the airfoil frame. The local circulation distribution over the airfoil is obtained from a Fourier series:

$$\gamma(\theta,t)=2U_\infty\left[A_0(t)\frac{1+\cos\theta}{\sin\theta}+\sum_{n=1}^{\infty}A_n(t)\sin n\theta\right] \quad (1)$$

with $A_0(t)$, … , $A_n(t)$ the time-dependant Fourier coefficients, c the airfoil chord and where:

$$x=\frac{c}{2}(1-\cos\theta) \quad (2)$$

The Kutta condition is enforced through the form of the Fourier series. The Fourier coefficients are determined from the instantaneous local downwash $w(\theta,t)$ by enforcing the potential flow boundary condition that the velocity is tangential to the airfoil surface:

$$A_0(t)=-\frac{1}{\pi}\int_0^\pi\frac{w(\theta,t)}{U_\infty}d\theta \quad (3)$$

$$A_n(t)=\frac{2}{\pi}\int_0^\pi\frac{w(\theta,t)}{U_\infty}\cos n\theta\,d\theta \quad (4)$$

where $w(\theta,t)$ is the velocity normal to the airfoil calculated from the motion kinematics:

$$\begin{aligned}w(\theta,t)=\frac{\partial\eta}{\partial x}\left(U_\infty\cos\alpha+\dot{h}\sin\alpha+\frac{\partial\Phi_{TEV}}{\partial x}+\frac{\partial\Phi_{LEV}}{\partial x}\right)\\ -U_\infty\sin\alpha-\dot{\alpha}(x-x_p)-\dot{h}\cos\alpha\\ -\frac{\partial\Phi_{TEV}}{\partial x}-\frac{\partial\Phi_{LEV}}{\partial x}\end{aligned} \quad (5)$$

with Φ_{TEV}, Φ_{LEV} the velocity potentials associated with the leading edge and trailing edge vortices, η the airfoil mean camber line and x_p the pivot position. At each time step, if the flow around the airfoil is attached, a trailing edge vortex (TEV) is released and advected by the flow at the following time step. However, a separation model is needed for large values of the angle of attack. The separation on the airfoil is obtained with an inviscid parameter developed by [18]. The Leading Edge Suction Parameter (LESP) is a non-dimensional measure of the suction at the leading edge, and equates the first Fourier coefficient:

$$\mathrm{LESP}(t)=A_0(t) \quad (6)$$

The critical value LESP_{crit} corresponds to the A_0 value associated with the angle of attack for which spikes appear in the negative part of the friction coefficient, near the leading edge. It is a measure of the maximum suction that a given airfoil can bear before separation and is independent of the motion. Beyond that LESP_{crit} value, the airfoil suction side boundary layer separates from the leading edge, which corresponds to the release of a leading edge vortex (LEV). In that case, there is shedding of both a TEV and a LEV. These vortices, at every time step, must enforce Kelvin's circulation theorem:

$$\Gamma_B(t)+\sum_{k=1}^{i}\Gamma_{TEV,k}+\sum_{l=1}^{i}\Gamma_{LEV,l}=0 \quad (7)$$

with the airfoil bound circulation:

$$\Gamma_B(t)=\int_0^\pi\gamma(\theta,t)d\theta=U_\infty c\pi\left[A_0(t)+\frac{A_1(t)}{2}\right] \quad (8)$$

The previous variables are written in a non-dimensional form for the fluid mechanics problem as:

$$w^* = \frac{w}{U_\infty} \quad U^* = \frac{w}{U_\infty} \quad W^* = \frac{W}{U_\infty}$$
$$X^* = \frac{X}{c} \quad Z^* = \frac{Z}{c} \quad \Gamma^* = \frac{\Gamma}{U_\infty c} \tag{9}$$

The velocity induced by a given vortex is described with the model of Vatistas which incorporates a finite core radius r_c [24].

$$U_k^* = \frac{\Gamma_k^*}{2\pi} \frac{Z^* - Z_k^*}{\sqrt{\left[\left(X^* - X_k^*\right)^2 + \left(Z^* - Z_k^*\right)^2\right]^2 + r_c^{*4}}}$$
$$W_k^* = -\frac{\Gamma_k^*}{2\pi} \frac{X^* - X_k^*}{\sqrt{\left[\left(X^* - X_k^*\right)^2 + \left(Z^* - Z_k^*\right)^2\right]^2 + r_c^{*4}}} \tag{10}$$

The non-dimensional time step is:

$$\delta t^* = \frac{\delta t U_\infty}{c} = 0.015 \tag{11}$$

The vortex core radius is taken to be 1.3 times the average spacing between the vortices [25]:

$$r_c^* = \frac{r_c}{c} = 1.3\delta t^* \tag{12}$$

The last shed vortex is placed at one third of the distance from the shedding edge to the previously shed vortex [15]:

$$X_{TEV,k}^* = X_{TE}^* + \frac{1}{3}\left(X_{TEV,k-1}^* - X_{TE}^*\right)$$
$$Z_{TEV,k}^* = Z_{TE}^* + \frac{1}{3}\left(Z_{TEV,k-1}^* - Z_{TE}^*\right)$$
$$X_{LEV,l}^* = X_{LE}^* + \frac{1}{3}\left(X_{LEV,l-1}^* - X_{LE}^*\right) \tag{13}$$
$$Z_{LEV,l}^* = Z_{LE}^* + \frac{1}{3}\left(Z_{LEV,l-1}^* - Z_{LE}^*\right)$$

For each time-step, the unknown parameters are the circulations corresponding to the newly shed vortices, advected by the velocity field. Firstly, if there is only a TEV shed at the iteration *i*, equation (5) is reduced to:

$$w^*\left(\theta, t_i^*\right) = T_1 + \Gamma_{TEV,i}^* T_2 \tag{14}$$

where T_1 and T_2 are terms depending on the angle of attack, the vertical displacement and the summation of the influence of the previously shed vortices. The only unknown parameter is the circulation of the TEV shed at iteration *i*. The airfoil bound circulation is obtained from (8) substituting the Fourier coefficients:

$$\Gamma_B^* = \int_0^\pi T_1\left(\cos\theta - 1\right)d\theta + \Gamma_{TEV,i}^* \int_0^\pi T_2\left(\cos\theta - 1\right)d\theta$$
$$= I_1 + I_2 \Gamma_{TEV,i}^* \tag{15}$$

where I_1 and I_2 are terms resulting of the integrals of T_1 and T_2. Substituting (15) into Kelvin's theorem (7):

$$\Gamma_{TEV,i}^* = -\frac{I_1 + \sum_{k=1}^{i-1} \Gamma_{TEV,k}^* + \sum_{l=1}^{i-1} \Gamma_{TEV,l}^*}{1 + I_2} \tag{16}$$

Secondly, if both a TEV and LEV are shed at iteration *i*, then equation (5) is reduced to:

$$w^*\left(\theta, t_i^*\right) = T_1 + \Gamma_{TEV,i}^* T_2 + \Gamma_{LEV,i}^* T_3 \tag{17}$$

where T_1, T_2 and T_3 are terms depending on the angle of attack, the vertical displacement and the summation of the influence of the previously shed vortices. There is two unknown parameters which are the circulations of the TEV and LEV shed at iteration *i*, requiring two equations. The airfoil bound circulation is obtained from (8) substituting the Fourier coefficients:

$$\Gamma_B^* = I_1 + I_2 \Gamma_{TEV,i}^* + I_3 \Gamma_{LEV,i}^* \tag{18}$$

where I_1, I_2 and I_3 are terms resulting of the integrals of T_1, T_2 and T_3. Kelvin's theorem (7) and the criterion on the critical LESP provide:

$$\Gamma_B^* + \Gamma_{TEV,i}^* + \Gamma_{LEV,i}^* + \sum_{k=1}^{i-1} \Gamma_{TEV,k}^* + \sum_{l=1}^{i-1} \Gamma_{LEV,l}^* = 0$$
$$A_0 - \mathrm{LESP}_{crit} = 0 \tag{19}$$

Substituting the bound circulation and the value of A_0, equation (19) is:

$$I_1 + \Gamma_{TEV,i}^*\left(1 + I_2\right) + \Gamma_{LEV,i}^*\left(1 + I_3\right) + \sum_{k=1}^{i-1} \Gamma_{TEV,k}^*$$
$$+ \sum_{l=1}^{i-1} \Gamma_{LEV,l}^* = 0 \tag{20}$$
$$J_1 + J_2 \Gamma_{TEV,i}^* + J_3 \Gamma_{LEV,i}^* - \mathrm{LESP}_{crit} = 0$$

Note that this is a linear system, and no iteration scheme is required as previously mentioned in [18] and [23]. Therefore, a significant gain in calculation time is expected [26]. As only the shed LEV and TEV are computed with the method, it is worth noticing that the simulation time is increasing with the number of vortices. In order to reduce that number, the vortices located four chords downstream of the leading edge can be amalgamated into larger structures [27]. That clustering can be realized with a multidimensional binary search tree or *k*-d tree [28], for all the vortices downstream of four chord of the airfoil.

The unsteady form of the Bernoulli theorem is used to calculate the pressure distribution along the airfoil:

$$p_{ps} - p_{ss} = \rho\left[\frac{1}{2}\left(V_{t,ss}^2 - V_{t,ps}^2\right) + \frac{\partial \Phi_{ss}}{\partial t} - \frac{\partial \Phi_{ps}}{\partial t}\right] \tag{21}$$

with the indices *ps* and *ss* respectively for the pressure side and suction side and V_t the tangential velocity. As the flow potential function is the sum of the potential functions of the bound circulation, TEV and LEV:

$$\Phi = \Phi_B + \Phi_{TEV} + \Phi_{LEV} \tag{22}$$

the tangential velocity is:

$$V_{t,ss} = U_\infty \cos\alpha + \dot{h}\sin\alpha + \left(\frac{\partial \Phi_B}{\partial x}\right)_{ss}$$
$$+ \left(\frac{\partial \Phi_{TEV}}{\partial x}\right)_{ss} + \left(\frac{\partial \Phi_{LEV}}{\partial x}\right)_{ss} \tag{23}$$

$$V_{t,ps} = U_\infty \cos\alpha + \dot{h}\sin\alpha + \left(\frac{\partial \Phi_B}{\partial x}\right)_{ps} + \left(\frac{\partial \Phi_{TEV}}{\partial x}\right)_{ps} + \left(\frac{\partial \Phi_{LEV}}{\partial x}\right)_{ps} \quad (24)$$

From the thin airfoil theory:

$$\left(\frac{\partial \Phi_B}{\partial x}\right)_{ss} = \frac{\gamma(x,t)}{2} \qquad \left(\frac{\partial \Phi_B}{\partial x}\right)_{ps} = -\frac{\gamma(x,t)}{2} \quad (25)$$

Then:

$$V_{t,ss}^2 - V_{t,ps}^2 = 2\left[U_\infty \cos\alpha + \dot{h}\sin\alpha + \frac{\partial \Phi_{TEV}}{\partial x} + \frac{\partial \Phi_{LEV}}{\partial x}\right]\gamma(x,t) \quad (26)$$

The potential functions time derivatives are:

$$\frac{\partial \Phi_{ss}}{\partial t} - \frac{\partial \Phi_{ps}}{\partial t} = \frac{\partial}{\partial t}\int_0^x \gamma(\xi,t)d\xi \quad (27)$$

Hence (21) becomes:

$$p_{ps} - p_{ss} = \rho\left\{\left[U_\infty \cos\alpha + \dot{h}\sin\alpha + \frac{\partial \Phi_{TEV}}{\partial x} + \frac{\partial \Phi_{LEV}}{\partial x}\right]\gamma(x) + \frac{\partial}{\partial t}\int_0^x \gamma(\xi,t)d\xi\right\} \quad (28)$$

The normal force on the airfoil is obtained:

$$F_N = \rho\left[\int_0^c \left(U_\infty \cos\alpha + \dot{h}\sin\alpha + \frac{\partial \Phi_{TEV}}{\partial x} + \frac{\partial \Phi_{LEV}}{\partial x}\right)\gamma(x,t)d\xi + \int_0^c \frac{\partial}{\partial t}\int_0^x \gamma(\xi,t)d\xi dx\right] \quad (29)$$

Using the Fourier coefficients, it is reduced to:

$$F_N = \rho U_\infty c\pi\left[\left(U_\infty \cos\alpha + \dot{h}\sin\alpha\right)\left(A_0 + \frac{A_1}{2}\right) + c\left(\frac{3\dot{A}_0}{4} + \frac{\dot{A}_1}{4} + \frac{\dot{A}_2}{8}\right) + \rho\int_0^c \left(\frac{\partial \Phi_{TEV}}{\partial x} + \frac{\partial \Phi_{LEV}}{\partial x}\right)\gamma(x,t)dx\right] \quad (30)$$

The axial force is given by the Blasius formula [23]:

$$F_A = \rho U_\infty^2 c\pi A_0^2 \quad (31)$$

Similarly, the moment about the position x_{ref} on the airfoil is:

$$M = x_{ref}F_N - \rho U_\infty c^2\pi\left[\left(U_\infty \cos\alpha + \dot{h}\sin\alpha\right)\left(\frac{A_0}{4} + \frac{A_1}{4} - \frac{A_2}{8}\right) + c\left(\frac{7\dot{A}_0}{16} + \frac{3\dot{A}_1}{16} + \frac{\dot{A}_2}{16} - \frac{\dot{A}_3}{64}\right) - \rho\int_0^c \left(\frac{\partial \Phi_{TEV}}{\partial x} + \frac{\partial \Phi_{LEV}}{\partial x}\right)\gamma(x,t)xdx\right] \quad (32)$$

The method can also be adapted to study the aerodynamic interaction between two airfoils [29].

3. FLUID-STRUCTURE INTERACTION

3.1. Structural model

As the classical flutter consists in a twisting mode and a bending mode, it is a three-dimensional instability. However, a two-dimensional modeling is often used to understand complex phenomena as limit cycle oscillations (LCO) [1, 5, 20, 30]. Figure 2 shows the two-dimensional airfoil and the relevant points: the aerodynamic center (AC), the elastic center (EC) and the center of gravity (CG). The distance ℓ is the distance between EC and AC, h the displacement in the direction orthogonal to the upstream velocity and α the angle of attack. The dynamic behavior of the airfoil is then reduced to its first twisting and bending mode, modeled respectively by a translation degree of freedom along Z and a rotation degree of freedom around the elastic axis passing through EC. In an airfoil, CG and EC are not generally superimposed. The eccentricity d of the center of gravity from the elastic center makes the coupling between twisting and bending motions.

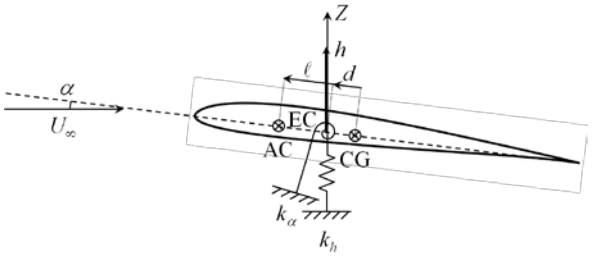

Figure 2. Structural model of the airfoil.

3.2. Coupling equations

The governing equations of the airfoil presented in figure 2 are [5, 20, 21]:

$$\begin{aligned} m\ddot{h} + k_h h + md\ddot{\alpha} &= L \\ J_{EC}\ddot{\alpha} + k_\alpha \alpha + md\ddot{h} &= M_{EC} \end{aligned} \quad (33)$$

with

$$M_{EC} = L\ell\cos\alpha + D\ell\sin\alpha + M_{AC} \quad (34)$$

and m the airfoil mass, J_{EC} the moment of inertia at the elastic center, k_h the equivalent flexural stiffness, k_α the equivalent twisting stiffness, L the lift and M_{EC} the elastic center pitching moment (Figure 2). Note that the structural problem is dimensional. A structural damping ξ can be considered [5] using the coupled eigenvalues ($w_{1,c}$, $w_{2,c}$) for null velocity of both modes:

$$\begin{aligned} m\ddot{h} + k_z h + md\ddot{\alpha} + 2\xi w_{1,c} m\dot{h} &= L \\ J_{EC}\ddot{\alpha} + k_\alpha \alpha + md\ddot{h} + 2\xi w_{2,c} J_{EC}\dot{\alpha} &= M_{EC} \end{aligned} \quad (35)$$

where the uncoupled eigenfrequencies for both modes are:

$$f_{1,d} = \frac{w_{1,d}}{2\pi} = \frac{1}{2\pi}\sqrt{\frac{k_z}{m}} \qquad f_{2,d} = \frac{w_{2,d}}{2\pi} = \frac{1}{2\pi}\sqrt{\frac{k_\alpha}{J_{EC}}} \quad (36)$$

Equation (35) can be rewritten in matrix form:

$$[M]\ddot{U} + [C]\dot{U} + [K]U = F \tag{37}$$

with the vectors:

$$U = \begin{pmatrix} h \\ \alpha \end{pmatrix} \qquad F = \begin{pmatrix} L \\ M_{EC} \end{pmatrix} \tag{38}$$

and the structural matrices:

$$[M] = \begin{pmatrix} m & md \\ md & J_{EC} \end{pmatrix} \quad [C] = 2\xi \begin{pmatrix} w_{1,c} m & 0 \\ 0 & w_{2,c} J_{EC} \end{pmatrix} \quad [K] = \begin{pmatrix} k_z & 0 \\ 0 & k_\alpha \end{pmatrix} \tag{39}$$

3.3. Coupling method

The fluid and structure equations are solved in a single code with a direct loose coupling, whose flow chart is presented in Figure 3. As previously mentioned, the non-dimensional time step δt^* is set to 0.015 for fluid LDVM computation, while the dimensional time step $\delta t = \delta t^* c / U_\infty$ is adjusted for each upstream velocity. For each simulation, 3000 LDVM time steps are computed to establish the flow around the airfoil and to advect the starting vortex downstream. The coupling is performed on the following 12000 time steps, computing for each time step, the lift and moment, which are input data for equations (33) solved by the method of Newmark [31]. Hereafter, the scheme is chosen implicit with standard values $\beta = 1/4$ and $\gamma = 1/2$. The resulting values of vector U are the new input values of the LDVM for the next time step. At that time, the method does not used internal iterations for solving the structural governing equations which necessitate to verify that δt is sufficiently small to converge towards the proper solution.

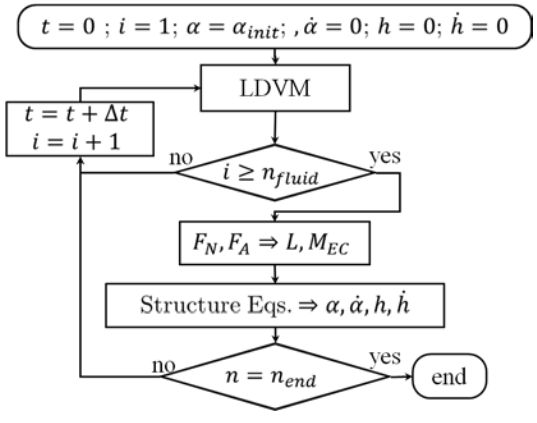

Figure 3. Flow chart of the fluid structure coupling.

3.4. Standard aeroelastic solutions

In order to compare the present method with classical aeroelastic solutions, several analytical methods are implemented. The aeroelastic equations (37) can be solved with various analytical expressions of lift and moment. The simplest model is the quasi-steady lift and pitching moment model:

$$L = \pi\rho U_\infty^2 c\left(\alpha - \frac{h}{U_\infty}\right) \qquad M_{AC} = \frac{1}{2}\rho U_\infty^2 c^2 C_{M,AC} \tag{40}$$

Due to the small angle of attack approximation, the drag is generally assumed to be null. More sophisticated expressions can be found in [32]. Theodorsen [7] showed that for unsteady aerodynamics and for small harmonic oscillations, the lift and pitching moment are:

$$L = \pi\rho U_\infty^2 c C(f_r)\left[-h + \left(\frac{3c}{4} - \ell\right)\alpha + U_\infty \alpha\right] + \frac{1}{4}\pi\rho c^2\left[-h + \left(\frac{c}{4} - \ell\right)\alpha + U_\infty \alpha\right] \tag{41}$$

$$M_{AC} = -\frac{1}{8}\pi\rho c^3\left[-\frac{1}{2}h + \frac{1}{2}\left(\frac{3c}{4} - \ell\right)\alpha + U_\infty \alpha\right] \tag{42}$$

where $C(f_r)$ is the Theodorsen function. The resolution of (37) with this model cannot be directly computed because the value of the $C(f_r)$ function is dependant from the reduced frequency f_r of the solution. A way to work around this issue is, for example, to compute iteratively the solution with the so-called *p-k* method or *k*-method. Another way to solve this problem is to replace the $C(f_r)$ function with an approximation of the induced flow velocity. This method introduced by Peters [33] is based on the following equation for lift, the moment equation (42) being unchanged:

$$L = \pi\rho U_\infty^2 c\left[-h + \left(\frac{3c}{4} - \ell\right)\alpha + U_\infty \alpha - \lambda_0\right] + \frac{1}{4}\pi\rho c^2\left[-h + \left(\frac{c}{4} - \ell\right)\alpha + U_\infty \alpha\right] \tag{43}$$

where λ_0 is the induced flow velocity. This new parameter is approximated using N_s induced flow states by:

$$\lambda_0 \approx \frac{1}{2}\sum_{n=1}^{N_s} b_n \lambda_n \tag{44}$$

with:

$$b_n = \begin{cases} (-1)^{n-1}\dfrac{(N_s + n + 1)!}{(N_s - n + 1)!\,n!^2} & \text{if } n \neq N_s \\ (-1)^{n-1} & \text{if } n = N_s \end{cases} \tag{45}$$

Each induced flow state can be determined using complementary first order ordinary differential equations [21]:

$$\vec{\vec{A}}\,\dot{\vec{\lambda}} + 2\frac{U_\infty}{c}\vec{\lambda} = \left[-h + \left(\frac{c}{2} - \ell\right)\alpha + U_\infty \alpha\right]\vec{c} \tag{46}$$

where:

$$\vec{\vec{A}} = \vec{\vec{D}} + \vec{d} \otimes \vec{b}^T + \vec{c} \otimes \vec{d}^T + \frac{1}{2}\vec{c} \otimes \vec{b}^T \tag{47}$$

$$D_{nm} = \begin{cases} \frac{1}{2}n & \text{if } n = m+1 \\ -\frac{1}{2}n & \text{if } n = m-1 \\ 0 & \text{if } n \neq m \pm 1 \end{cases} \quad (48)$$

$$d_n = \begin{cases} \frac{1}{2} & \text{if } n = 1 \\ 0 & \text{if } n \neq 1 \end{cases} \quad (49)$$

$$c_n = \frac{2}{n} \quad (50)$$

The ordinary differential equations (37) and (46) are then rewritten in the form of a new matrix form:

$$[M_\lambda]\dot{\vec{U}}_\lambda + [C_\lambda]\ddot{\vec{U}}_\lambda + [K_\lambda]\vec{U}_\lambda = \vec{F}_\lambda \quad (51)$$

with:

$$\vec{U}_\lambda^T = \begin{pmatrix} h & \alpha & \lambda_1 & \cdots & \lambda_{N,s} \end{pmatrix} \quad (52)$$

The problem can be solved classically as a generalized eigenvalue problem.

4. RESULTS

Hereafter, a SD7003 is considered because the development of $LESP_{crit}$ with Reynolds number is available for this airfoil. In the present work, the structural linear data correspond to a light aircraft wing [5] with $m = 140$ kg·m^{-1}, $d = 0.5$ m, $J_{EC} = 45$ kg·m, $k_z = 22000$ N·m^{-2}, $k_\alpha = 30000$ N·rad^{-1} and a structural damping $\xi = 0.01$. The airfoil initial angle of attack is 1°. The different cases discussed hereafter depend on the upstream flow velocity U_∞. which is varied between 50 and 80 m·s^{-1}.

Figure 4-a presents the time evolution of the airfoil displacement h along axis Z and of its angle of attack α for an upstream velocity of 50 m·s^{-1}. The 3000 initial time steps, corresponding to LDVM computations without structural coupling, are not plotted. The converging behavior is clearly observed with a stabilization around a position $h = 0.05$ m and an angle of attack $\alpha = 1.5°$. For a larger velocity $U_\infty = 65$ m·s^{-1} (figure 4-b), the airfoil is diverging and a limit cycle oscillation (LCO) is observed beyond the airfoil stall.

Figure 5-a presents the lift, drag and moment coefficient at the elastic center for an upstream velocity of 50 m·s^{-1}. From the establishment of the coupling, large modulations of the aerodynamic coefficients are observed, but they are rapidly converging toward a steady state. The wing behavior is completely different for $U_\infty = 65$ m·s^{-1} (figure 5-b), with an increase of the amplitude of the coefficients up to a saturation, corresponding to a LCO in the phase portrait.

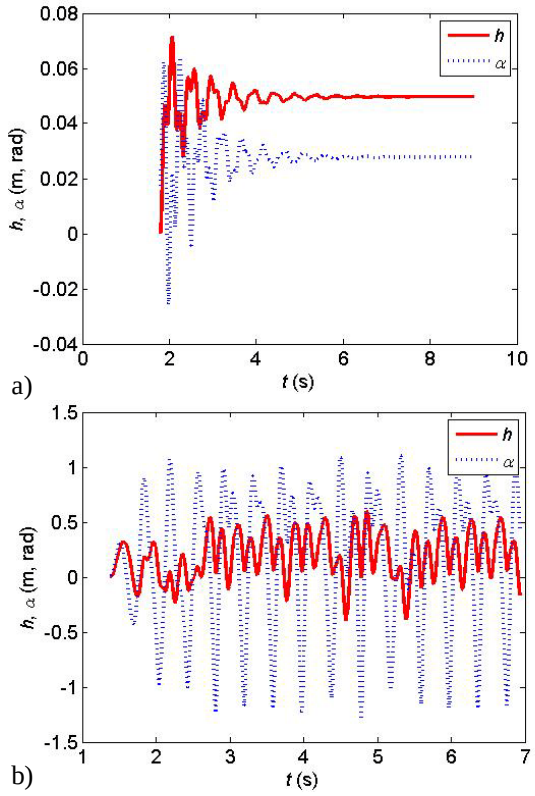

Figure 4. Time evolution of the airfoil displacement and angle of attack corresponding to a) $U_\infty = 50$ m·s^{-1} and b) $U_\infty = 65$ m·s^{-1}.

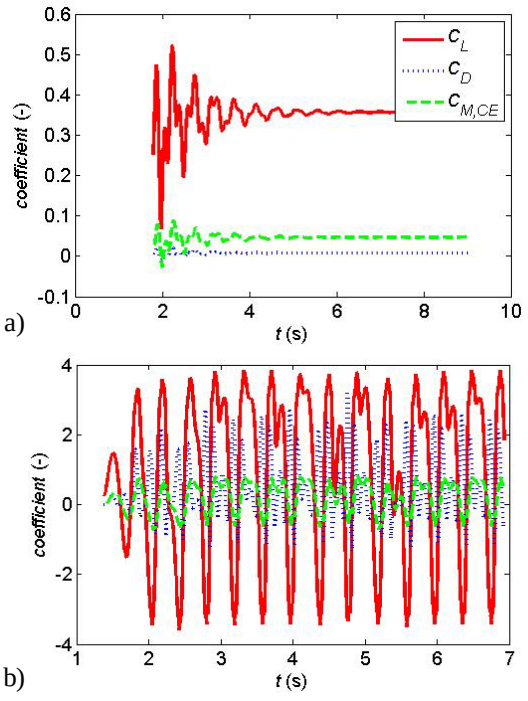

Figure 5. Time evolution of the aerodynamic coefficients corresponding to a) $U_\infty = 50$ m·s^{-1} and b) $U_\infty = 65$ m·s^{-1}.

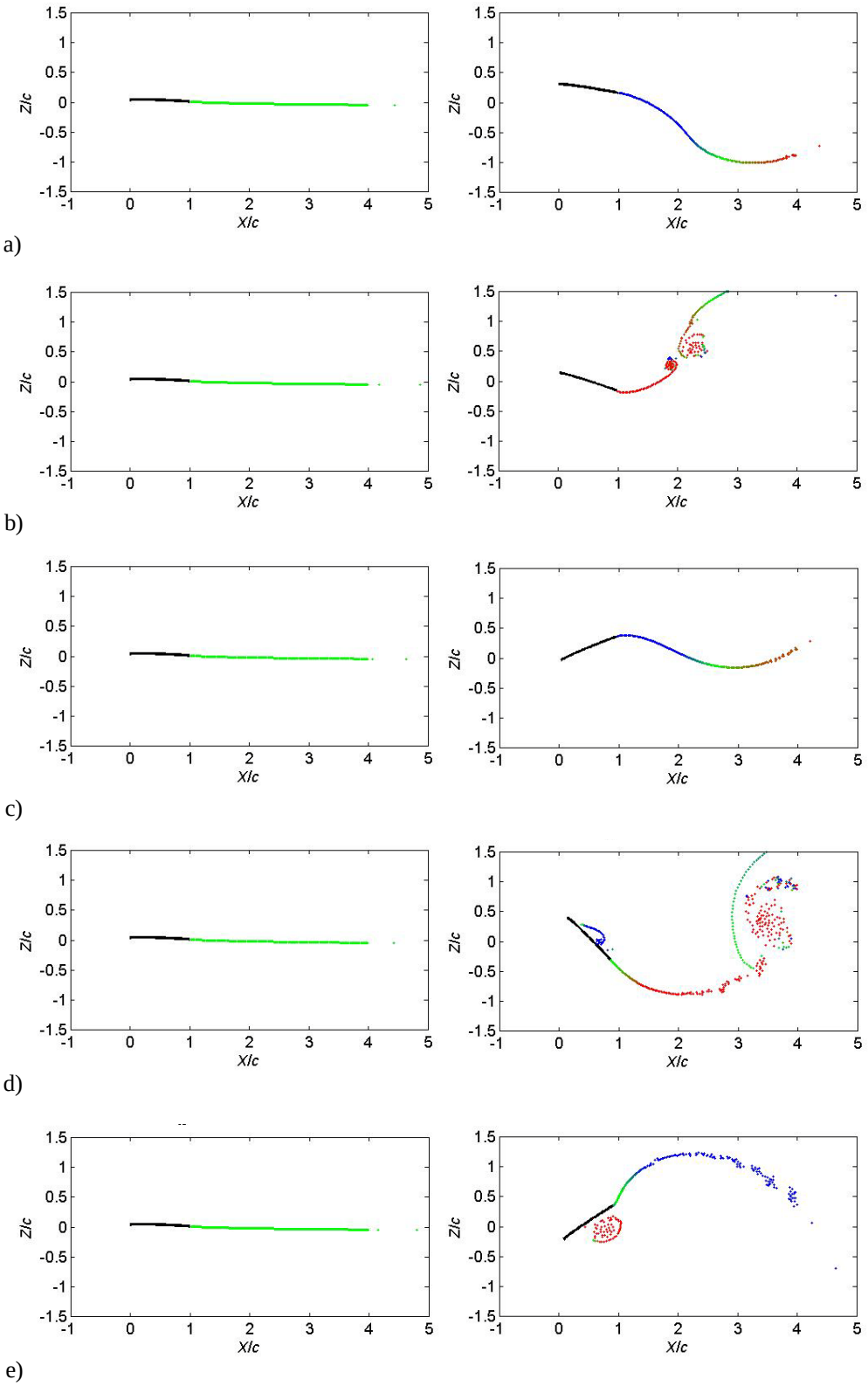

Figure 6. Airfoil position for U_∞ = 50 m·s^{-1} (left, converging motion) and for U_∞ = 65 m·s^{-1} (right, diverging motion) and vortex shedding circulation (negative in blue, around zero in green and positive in red) for different times: a) t = 5 s, b) t = 5.25 s, c) t = 5.5 s, d) t = 5.75 s, e) t = 6 s.

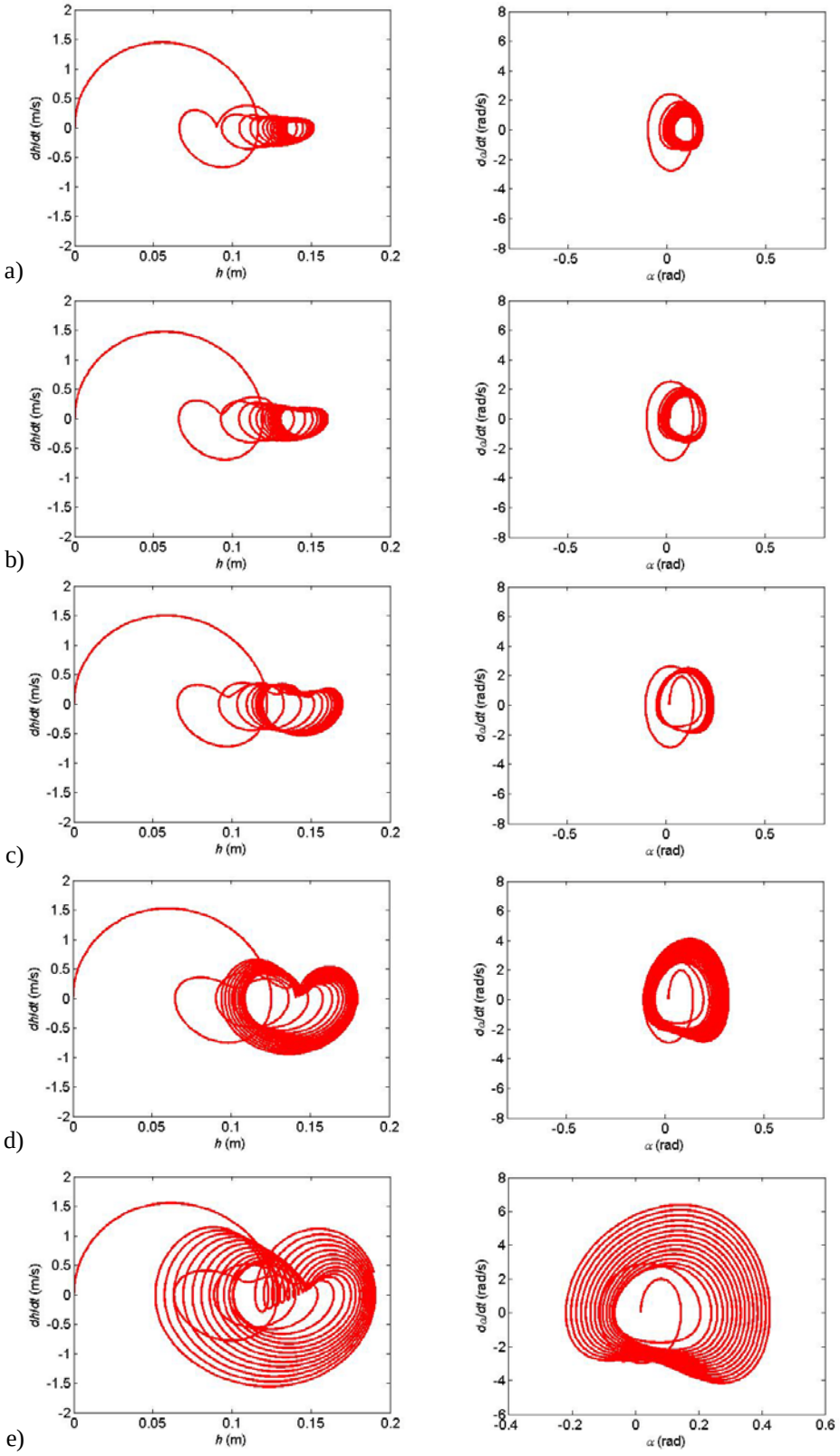

Figure 7. Phase portrait of the vertical airfoil motion h (left) and of the angle of attack α (right) for cases corresponding to upstream velocity: a) $U_\infty = 58.1\ \mathrm{m{\cdot}s^{-1}}$, b) $U_\infty = 58.3\ \mathrm{m{\cdot}s^{-1}}$, c) $U_\infty = 58.5\ \mathrm{m{\cdot}s^{-1}}$, d) $U_\infty = 58.7\ \mathrm{m{\cdot}s^{-1}}$, e) $U_\infty = 58.9\ \mathrm{m{\cdot}s^{-1}}$.

The time development of the airfoil motion and flow vortices is presented in figure 6, for the velocities

previously discussed $U_\infty = 50$ m·s^{-1} and $U_\infty = 65$ m·s^{-1}. These times are taken after the initiation of fluid-structure coupling. For $U_\infty = 50$ m·s^{-1} (figure 6, left), the flow is completely attached, no TEV is created and the airfoil is stable. On the contrary, for $U_\infty = 65$ m·s^{-1} (figure 6, right), the airfoil presents large modulations in its position and angle of attack, associated with changes in its global circulation and resulting in the emission of a trailing vortex (figure 6-b). A possible detached flow on the suction side (figure 6-d) or on the pressure side (figure 6-e) is also able to occur.

Figure 7 presents the phase portrait of the vertical airfoil motion h and of the angle of attack α for cases corresponding to upstream velocities between 58 and 59 m·s^{-1}, in order to track the critical speed of the system. Figures 7-a,b show converging paths in the phase plane toward a point, corresponding to stable cases. Figures 7-c,d,e present diverging paths associated to unstable airfoil coupling. The velocity threshold between these two behaviors is found around 58.4 m·s^{-1}. An aeroelastic computation of the critical speed with quasi-steady aerodynamics (eqs. 41-42) provides a value of 57.5 m·s^{-1}. The computation of the critical speed with the model of Peters [33] in eq. (51) provides a value of 60.5 m·s^{-1}. That value is to compared to the critical speed of 58.4 m·s^{-1} obtained by the present fluid-structure coupling method. These estimates of the critical speed lead to reduced frequencies of the order of one using equation (36), which is the case of a strong fluid-structure interaction in the actual configuration.

Figure 8 presents the phase portrait of the vertical airfoil motion h and of the angle of attack α for an upstream velocity of 80 m·s^{-1}, with the associated LCO.

5. CONCLUSION

The LDVM is a reduced order method that has been successfully implemented previously to predict flow detachment and aerodynamic forces on an airfoil. In this paper, a loose coupling with a structural model is implemented. The coupling equations are solved by the method of Newmark. The LDVM is first computed to advect the starting vortex far away from the airfoil. Then, for each time step, LDVM provides the aerodynamic coefficients and pitching moment which are input data for the structural equations, leading to a change in the airfoil position and angle of attack. The coupling method is applied to a straight wing build on a SD7003 airfoil with structural linear data corresponding to a light aircraft configuration. Asymptotically stable or unstable behaviors are found depending on the control parameter which is the upstream flow velocity. In order to track the critical speed, phase portraits of the vertical airfoil displacement and of the angle of attack are built. A change from a converging path in the phase portrait toward a point to a diverging path is found for velocities larger than the flutter speed of 58.4 m·s^{-1}. This result is close to the value of 57.5 m·s^{-1} obtained with a purely quasi-steady model or 60.5 m·s^{-1} obtained by the model of Peters. These results are validating the present coupling method. Above this flutter speed, LCO are highlighted due to the ability of the method to predict the detached flow on the suction side and on the pressure side. It is one of the main interests of the proposed method. In the future, it will be compared to experimental case of LCO.

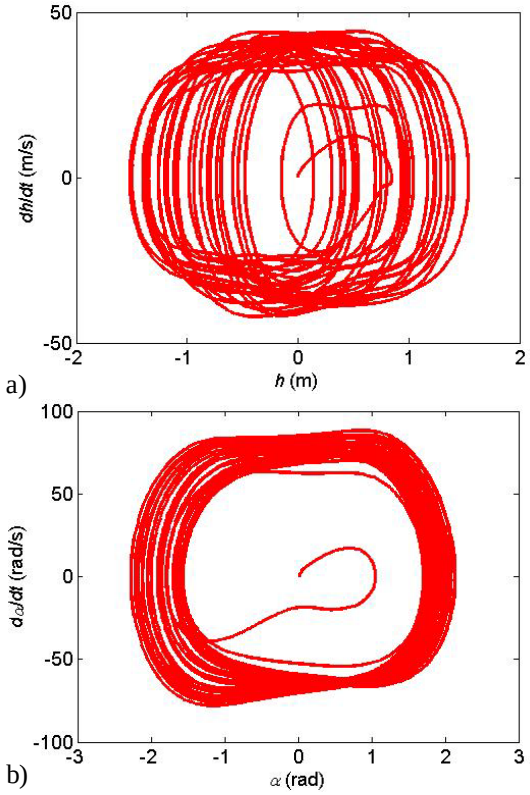

Figure 8. Phase portrait of the vertical airfoil motion h (left) and of the angle of attack α (right) for cases corresponding to upstream velocity: a) $U_\infty = 80$ m·s^{-1}.

6. REFERENCES

1. Hémon, P. (2006) *Vibrations des structures couplées avec le vent*, Éditions de l'École Polytechnique.
2. Munk, M. (1922) *General theory of thin wing sections*, Tech. rep., 142 NACA.
3. Birnbaum, W. (1923) Die tragende Wirbel fläche als Hilfsmittel zur Behandlung des ebenen Problems der Tragflügeltheorie, *ZAMM-Journal of Applied Mathematics and Mechanics/Zeitschrift für Angewandte Mathematik und Mechanik* 3(4):290-297.
4. Glauert, H. (1926) *The elements of aerofoil and airscrew theory*, Cambridge University Press.

5. Axisa, F. (2001) *Vibrations sous écoulements*, Hermes Science Publications.
6. Wagner, H. (1925) Über die Entstehung des dynamischen Auftriebes von Tragflügeln. *Z Angew Math Mech* 5 (1):17-35.
7. Theodorsen, T. (1935) *General theory of aerodynamic instability and the mechanism of flutter*, Tech. rep., 496 NACA.
8. Garrick, I.E. (1937) *Propulsion of a flapping and oscillating airfoil*, Tech. rep., NACA TN-D-85.
9. von Kármán, T. & Sears, W. (1938) Aerofoil theory for non-uniform motion, *Journal of Aeronautical Science* 5 (10):379-390.
10. Clements, R.R. (1973) An inviscid model of two-dimensional vortex shedding, *Journal of Fluid Mechanics* 57 (2):321-336.
11. Clements, R.R. & Maull, D.J. (1975) The representation of sheets of vorticity by discrete vortices, *Progress in Aerospace Science* 16 (2):129-146.
12. Kiya, M. & Arie, M. (1977) A contribution to an inviscid vortex-shedding model for an inclined at plate in uniform flow, *Journal of Fluid Mechanics* 82 (2):241-253.
13. Albano, E. & Rodden, W.P. (1969) A doublet lattice method for calculating lift distributions on oscillating surfaces in subsonic flow, *AIAA Journal*, 7 (2): 279-85.
14. Hedman, S.G. (1965) *Vortex lattice method for calculation of quasi steady state loadings on thin elastic wings in subsonic flow*, The Aeronautical Research Institute of Sweden, Report 105.
15. Ansari, S.A., Żbikowski, R. & Knowles, K. (2006) Nonlinear unsteady aerodynamic model for insect-like flapping wings in the hover. Part 1 methodology and analysis, *Proc. Inst. Mech. Engrs G*, 220 (3), 61-83.
16. Xia, X. & Mohseni, K. (2013) Lift evaluation of a two-dimensional pitching flat plate, *Physics of Fluids* 25:091901.
17. Hammer, P., Altman, A. & Eastep, F. (2014) Validation of a discrete vortex method for low Reynolds number unsteady flow, *AIAA Journal* 52 (3):643-649.
18. Ramesh, K., Gopalarathnam, A., Granlund, K., Ol, M.V. & Edwards, J.R. (2014) Discrete vortex method with novel shedding criterion for unsteady aerofoil flows with intermittent leading edge vortex shedding. *Journal of Fluid Mechanics*, 751: 500-538.
19. Ramesh, K., Granlund, K., Ol, M.V., Gopalarathnam, A. & Edwards, J.R. (2017) Leading-edge flow criticality as a governing factor in leading-edge vortex initiation in unsteady airfoil flows. *Theoretical and Computational Fluid Dynamics* pp 1-28.
20. Dowell, E.H. (2005) *A Modern Course in Aeroelasticity*, vol. 116, Dordrecht : Kluwer Academic Publishers.
21. Hodges, D.H. & Pierce, G.A. (2002) *Introduction to structural dynamics and aeroelasticity*, Cambridge.
22. Blanc, F. (2009) *Méthodes numériques pour l'aéroélasticité des surfaces de contrôle des avions*, Ph.D. thesis, Institut Supérieur de l'Aéronautique et de l'Espace.
23. Katz, J. & Plotkin, A. (2000) *Low-Speed Aerodynamics*, Cambridge University Press.
24. Vatistas, G.H., Kozel, V. & Mih, W.C. (1991) A simpler model for concentrated vortices, *Exp. Fluids*, 11 (1), 73-76.
25. Leonard, A. (1980) Vortex methods for flow simulations, *J. Comput. Phys.* 37 (3), 289-335.
26. Faure, T.M., Dumas, L., Drouet, V. & Montagnier, O. (2017) A modified discrete-vortex method with shedding criterion for unsteady or constant angle of attack flow prediction, *Theoretical and Computational Fluid Dynamics* (in review).
27. Sarpkaya, T. (1975) An inviscid model of two-dimensional vortex shedding for transient and asymptotically steady separated flow over an inclined plate, *Journal of Fluid Mechanics* 68 (1), 109-128.
28. Bentley, J.L. (1975) Multidimensional binary search trees used for associative searching, *Communications of the ACM*, 18 (9), 509-517.
29. Faure, T.M., Drouet, V. & Montagnier, O. (2017) Discrete vortex method for a detached flow on a two-airfoil configuration at high angle of attack, *52th 3AF International Conference on Applied Aerodynamics*, Lyon, France, 27 - 29 March 2017, paper FP07-AERO2017.
30. Murua, J. (2012) Applications of the unsteady vortex-lattice method in aircraft aeroelasticity and flight dynamics, *Progress in Aerospace Sciences* 55 (2012) 46-72.
31. Newmark, N.M. (1959) A method of computation for structural dynamics. *Journal of Engineering Mechanics*, ASCE, 85 (EM3) 67-94.
32. Fung, Y. C. (1969) *An introduction to the theory of aeroelasticity*. Dover Publications.
33. Peters, D.A. (2008) Two-dimensional incompressible unsteady airfoil theory—an overview, *Journal of Fluids and Structures*, 24 (3), 295–312.